

# Elliptical Fitting as an Alternative Approach to Complex Nonlinear Least Squares Regression for Modeling Electrochemical Impedance Spectroscopy

Norman Pfeiffer<sup>1</sup> <sup>a</sup>, Toni Wachter<sup>1</sup>, Jürgen Frickel<sup>2</sup>, Christian Hofmann<sup>1</sup>, Abdelhamid Errachid<sup>3</sup> and Albert Heuberger<sup>2</sup>

<sup>1</sup>Fraunhofer IIS, Fraunhofer Institute for Integrated Circuits, Am Wolfsmantel 33, 91058 Erlangen, Germany

<sup>2</sup>Lehrstuhl für Informationstechnik mit dem Schwerpunkt Kommunikationselektronik (LIKE), Friedrich-Alexander Universität Erlangen-Nürnberg, Am Wolfsmantel 33, 91058 Erlangen, Germany

<sup>3</sup>Institut des Sciences Analytiques, Université de Lyon, 5 rue de la Doua, 69100 Villeurbanne, France

**Keywords:** Electrochemical Impedance Spectroscopy, Elliptical Fitting, Randles Circuit, Least Squares Fitting, Charge Transfer Resistance, Complex Nonlinear Least Squares.

**Abstract:** Electrochemical impedance spectroscopy is an important procedure with the ability to describe a wide range of physical and chemical properties of electrochemical systems. The spectral behavior of impedimetric sensors is mostly described by the Randles circuit, whose parameters are determined by regression techniques on the basis of measured spectra. The charge transfer resistance as one of these parameters is often used as sensor response. In the laboratory environment, the regression is usually performed by commercial software, but for integrated, application-oriented solutions, separate approaches must be pursued. This work presents an approach for elliptical fitting of the curve in the Nyquist plot, which is compared to the complex nonlinear least squares (CNLS) regression technique. For this purpose, artificial spectra were generated, which were considered both with and without noise superposition. Although the average error in calculating the charge transfer resistance from noisy signals using the elliptical fitting of  $-2.7\%$  was worse than the CNLS with  $2.4 \cdot 10^{-2}\%$ , the former required only about  $1/225$  of the computing time compared to the latter. Following application-oriented evaluations of the achievable accuracies, the elliptical approach may turn out to be a resource saving alternative.

## 1 INTRODUCTION

Electrochemical impedance spectroscopy (EIS) is a common measurement technology for the analysis of biosensors, such as FET-based structures (Kharitonov et al., 2001). Its advantage is the description of chemical and physical phenomena of an electrochemical system, thus allows the characterization of the electrical properties of the sensor surface and the investigation of interfacial reaction mechanisms (Macdonald, 1990). Furthermore, impedimetric biosensors have other advantages such as label-free measurements, miniaturization capability, low production costs etc. (Prodromidis, 2010). In research EIS is used in various chemical and medical applications for the analysis of biosensors, e.g. for the diagnosis of heart dis-

eases (Halima et al., 2019) or of Alzheimer's disease (Rushworth et al., 2014), for the detection of bacteria as *Escherichia coli* or viruses (Leva-Bueno et al., 2020) or for detection of cancer cells (Chowdhury et al., 2018).

The application-oriented interpretation of the impedance spectra of biosensors is usually done by modeling the biofunctionalized sensor area. For this purpose an equivalent circuit diagram is applied, which describes the electrochemical and physical phenomena. As a model for an electrode in contact with an electrolyte, the so called Randles circuit is used, which describes a one-step charge transfer process involving the diffusion of reactants to the interface (Barsoukov and Macdonald, 2005). In the majority of published EIS studies, different interface parameters such as charge transfer resistance  $R_{ct}$  or double layer capacitance  $C_{dl}$  are determined by modeling

<sup>a</sup>  <https://orcid.org/0000-0002-6839-3002>

(Pejic and De Marco, 2006). Within the scope of scientific publications, commercial software is usually used to realize the modeling, which is performed by a complex nonlinear least squares (CNLS) regression technique (Kauffman, 2009) with the electrical equivalent circuit diagram. Alternatively,  $R_{ct}$  is determined manually at the second extrapolated intersection with the real axis on the low-frequency side of the Nyquist plot, thus by a geometric approach. This method for estimating  $R_{ct}$  is used extensively in the electrochemical field (Randviir and Banks, 2013).

Electrochemical biosensors can be used in a variety of applications, such as the examination of sweat, saliva, blood or urine as part of a wearable sensor (Sun et al., 2016) (Dang et al., 2018) (Sgobbi et al., 2016). Apart from medical applications, also small and energy-efficient devices for gas monitoring or environmental analysis are considered (Cimafonte et al., 2020) (Willa et al., 2017). Especially as soon as EIS is used in a mobile scenario, it must be determined where the evaluation of recorded spectra will be carried out. On the one hand, raw data can be sent to a computing unit, which, however, results in greater dependencies on the overall system architecture. An example of this are alarm systems, which have a higher risk of errors due to the communication link to the computing unit. On the other hand, modelling can be carried out directly on the (low-power) electronics. In the latter case the efficiency of algorithms plays an important role.

This work proposes an approach that uses elliptical fittings to provide an automated, geometric estimation of  $R_{ct}$ . Thus, reproducibilities and accuracies should be increased compared to manual methods, but lower computational times than CNLS are expected. Therefore both the elliptical fitting and CNLS were implemented in Python and evaluated by simulated data with and without noise.

## 2 MATERIALS AND METHODS

### 2.1 Generation of Simulation Data

As usual for FET-based biosensors, the Randles circuit was used to simulate the artificial impedance spectra. Its equivalent circuit consists of an electrolyte resistance  $R_s$  in series with a parallel circuit of the double layer capacitance  $C_{dl}$  and an impedance of the Faraday charge exchange. The latter is a serial connection of the charge transfer resistance  $R_{ct}$  and the Warburg impedance  $Z_w$ . The Faraday impedance has its origin in the ion exchange between the electrolyte and the ions in the metallic conducting elec-

trode (Yuan et al., 2010). In many cases the double layer capacitance  $C_{dl}$  is replaced by a constant phase element CPE due to non-ideal conditions such as porous electrodes. The impedance of the CPE is defined by

$$Z_{CPE}(f) = \frac{1}{Q(i2\pi f)^n} \quad n \in [0, 1]. \quad (1)$$

Here,  $Q$  is a pre-factor of the CPE and  $n$  its exponent. For  $n = 1$ , Equation 1 represents the behaviour of an ideal capacitor with the capacitance  $C = Q$  (Shoar Abouzari et al., 2009).

A special case of the CPE is  $Z_w$  with a constant phase of  $45^\circ$ . It describes the contribution of diffusion from or to an electrode. A theoretical electrode with an infinitely large area and thus unlimited diffusion can be described as follows

$$Z_w(f) = \frac{1}{Q_w \sqrt{(i2\pi f)}}. \quad (2)$$

The used equivalent circuit for providing a Randles circuit and therefore simulating the electrical behaviour of a FET-based biosensor is shown in Figure 1.

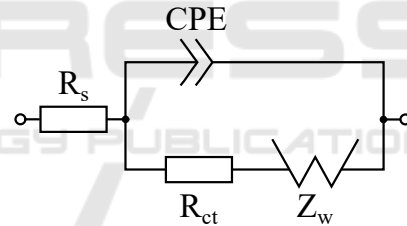


Figure 1: Equivalent circuit of the Randles circuit.  $R_s$  is the electrolyte resistance,  $R_{ct}$  charge transfer resistance,  $Z_w$  Warburg impedance,  $CPE$  constant phase element.

In order to achieve the expected shape of the Randles circuit in a Nyquist plot with a semicircle behaviour at higher frequencies and the impact of the Warburg impedance only in the lower-frequency half of the semicircle, the ranges for the parameter values were selected as presented in Table 1.

To simulate spectra for test purposes, random numbers for a factor  $a$  and an exponent  $b$  were drawn, resulting in a parameter  $\beta = a \cdot 10^b$  within the mentioned range of values for each component. These parameters are finally used to generate the artificial Randles circuit. However, depending on the relative ratio between the parameters of the spectrum, its Nyquist plot can assume the form of a simple line, since in this case  $Z_w$  can dominate the spectra. Based on the practical irrelevance of this case, such simulations are discarded by checking the change of its phase and comparing it with a threshold angle.

Table 1: Range of values for each parameter of the Randles circuit used to simulate artificial spectra.  $R_s$  electrolyte resistance,  $R_{ct}$  charge transfer resistance,  $Q_w$  pre-factor of the Warburg impedance  $Z_w$ ,  $Q$  pre-factor of the CPE,  $n$  exponent of the CPE.

Parameter	Min	Max	Unit
$R_s$	$10^3$	$10^5$	$\Omega$
$R_{ct}$	$10^4$	$9 \cdot 10^6$	$\Omega$
$Q_w$	$10^{-8}$	$10^{-6}$	$S \cdot \sqrt{s}$
$Q$	$10^{-11}$	$10^{-6}$	$S \cdot s^n$
$n$	0.5	1	-

Each simulation was run twice, once without and once with noise. For the latter a Gaussian noise was superimposed to the argument ( $\mu = 0$ ,  $\sigma^2 = 1\%$ ) and the phase ( $\mu = 0$ ,  $\sigma^2 = 1^\circ$ ). In total, 100 spectra were simulated, each without and with noise.

## 2.2 Complex Nonlinear Least-squares Regression

To determine the parameter  $R_{ct}$ , the parameters  $B$  of the equivalent circuit are calculated using the acquired values  $Z_{acq}$ . This was realised by using the method of least squares (LS). The LS is a mathematical standard procedure for the calculation of the parameters  $B = (\beta_1, \beta_2, \dots, \beta_n) \in \mathbb{R}^n$  of a system of equations. The goal of the procedure is to minimize the residuals  $r_m$  between the values of the model curve  $z_{mod}$  and the acquired data  $z_{acq}$  in respect to the measuring frequency  $f_m$ :

$$r_m(B) = z_{acq}(f_m) - z_{mod}(B, f_m) \quad (3)$$

Therefore the sum of the error squares  $R$  is defined as the sum of the least squares for all frequencies  $f_m = (f_1, f_2, \dots, f_M) \in \mathbb{R}^M$ :

$$R(B) = \frac{1}{2} \sum_{m=1}^M r_m(B)^2 \quad (4)$$

Those parameters  $B$  are to be found, which minimize the sum of the quadratic residuals:

$$R_{min} = \min_{B \in \mathbb{R}^M} \frac{1}{2} \sum_{m=1}^M r_m(B)^2 \quad (5)$$

The solution of this minimization problem depends on the type of model function (Papageorgiou et al., 2015). In the present case there is a nonlinear optimization problem, for which the Gauss-Newton method is a suitable procedure for the calculation of optimal parameters  $B$ . The method is a numerical approach to solve nonlinear minimization problems according to the LS. The basic idea is to linearize the

nonlinear cost function  $R$  and subsequently optimize it with the help of the LS. To achieve the linearization the first order Taylor expansion is used. For the residual  $r_m$  with the parameters  $B^{(k)} \in \mathbb{R}^N$  in iteration step  $k$  a linearization to

$$\tilde{r}_m(B, B^{(k)}) = r_m(B^{(k)}) + \nabla r_m(B^{(k)})^T (B - B^{(k)}) \quad (6)$$

with the Jacobi matrix  $J = \nabla r_m(B^{(k)})^T$  results. This leads to the minimization problem:

$$\begin{aligned} B^{(k+1)} &= \min_{B \in \mathbb{R}^M} \sum_{m=1}^M \tilde{r}_m(B, B^{(k)})^2 \\ &= B^{(k)} - ((J|_{B^{(k)}}) \cdot (J|_{B^{(k)}})^T)^{-1} (J|_{B^{(k)}}) \cdot R(B^{(k)}) \end{aligned} \quad (7)$$

This iteration step is repeated until the result converges (Bertsekas, 1999). To guarantee a minimization and to treat the case of a singular matrix  $JJ^T$ , the Gauss-Newton step can be optimized to

$$\begin{aligned} B^{(k+1)} &= B^{(k)} \\ &\quad - \alpha^{(k)} ((J|_{B^{(k)}}) \cdot (J|_{B^{(k)}})^T + \Delta^{(k)})^{-1} (J|_{B^{(k)}}) \cdot R(B^{(k)}) \end{aligned} \quad (8)$$

with  $\alpha^{(k)} \geq 0$ . Thereby  $\Delta^{(k)}$  is selected so that  $(J|_{B^{(k)}}) \cdot (J|_{B^{(k)}})^T + \Delta^{(k)}$  is positive definite. If  $\Delta^{(k)}$  is chosen as a positive multiple of the unit matrix  $\Delta^{(k)} = \lambda^k I$ ,  $\lambda \geq 0$  the Levenberg-Marquardt algorithm (LMA) is obtained (Bertsekas, 1999), which is applied in the present work to determine the component values of the equivalent circuit shown in Figure 1.

Since the first derivative of the equation describing the equivalent circuit is not known, the Jacobi matrix must be determined during the regression by numerical differentiation. Furthermore, due to the use of capacitors and resistors, the parameters of the equivalent circuit diagram have extreme differences in size, so that derivation is not straightforwardly possible. This is explained by the fact that the existing differences in the magnitude of the parameter values have an unequal strong influence on the numerical differentiation.

Furthermore, parameters of different magnitudes lead to problems during regression with the LMA. Within each iteration, the error between the measured value and the calculated value is evaluated and the influence of changing a single parameter is assessed. Accordingly the step size for each parameter is adapted within an iteration. However, a small step size of a resistor may have little to no influence on the calculated impedance value, whereas the same step size may be quite significant for a capacitance.

For these reasons, all parameters are normalized to a uniform value range. In a first step, each parameter  $\beta$  is divided into a factor  $a$  and an exponent  $b$ :

$$\beta = a \cdot 10^b \quad (9)$$

Consequently, the number of parameters is doubled. Then the parameters are scaled to the same value range  $W \in [t_1, t_2]$ :

$$\beta_{scaled} = t_1 + \frac{\beta - \min(\beta)}{\max(\beta) - \min(\beta)} \cdot (t_2 - t_1) \quad (10)$$

These parameters are then used to perform the regression.

The acquired impedances  $Z_{acq}$  and the calculated impedances  $Z_{cal}$  are also standardized, whereby these are separated into the real and imaginary parts. Thus the real and imaginary part have the same influence on the calculated error. This step is performed using a z-score:

$$z_{standard} = \frac{z - \bar{z}}{\sigma} \quad (11)$$

with the mean value  $\bar{z}$  and the standard deviation  $\sigma$ . For both impedances  $Z_{acq}$  and  $Z_{cal}$ ,  $\bar{z}$  and  $\sigma$  are calculated from  $Z_{acq}$ . The z-score is chosen because it does not show significant differences in empirical comparison to the min-max normalization using simulated data. However, it is generally better at handling outliers, which is relevant for real measured spectra.

Since CNLS is based on the LMA algorithm, the success of the procedure is strongly dependent on the used start parameters. By using unfavorable start parameters the algorithm could get stuck in a local optimum and does not find a satisfying result. In the ideal case, values close to the actual parameter sizes are chosen as start parameters. However, since the value ranges for each parameter are quite large, it is not possible to make a generally valid preselection. To address this issue, a pre-fit method that allows the estimation of favorable start values for CNLS has already been published (Barsukov and Macdonald, 2012).

In general, the approach of the pre-fit is to perform a CNLS with a circuit that contains a series connection of two RC elements ( $R_m, C_m$  for  $m = 1, 2$ ) and a series resistor  $R_0$  (see Figure 2). The result of the pre-fit is then used as the start value for the actual CNLS with the Randles circuit. Therefore, the components from the pre-fit have to be assigned to the components from the Randles circuit and can then be used as start values for the CNLS. For this purpose, the time constants of the determined RC elements are calculated according to  $\tau_m = R_m C_m$  and sorted by size in ascending order.

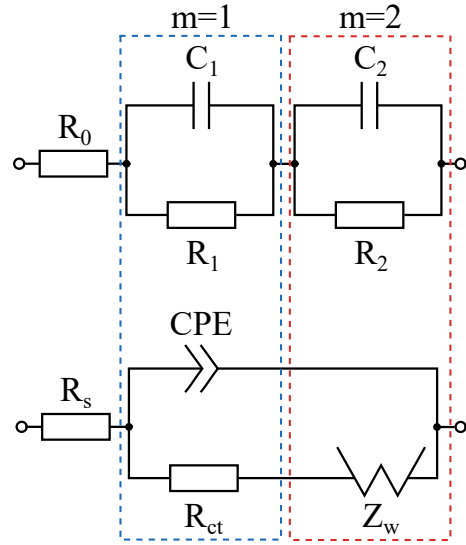


Figure 2: Equivalent circuit diagram of the pre-fit approach (top) with the corresponding assignment of the component values to the parts of the Randles circuit (bottom). The assignment is done by means of the time constant  $\tau_m$ .

Using the  $\tau_m$  sorted by size, the elements of the pre-fit can be assigned to the components of the Randles circuit. It is now exploited that  $\tau$  for diffusion is much larger than that of a charge exchange. First,  $R_s$  is given by the series resistance  $R_0$ . The remaining components of the Randles circuit are then assigned an ordinal number  $m$ . CPE and  $R_{ct}$  form  $m = 1$  and  $Z_w$  is assigned  $m = 2$ . This ordinal number corresponds to the time constants of the pre-fit, sorted by size.

Thus, the smaller time constant from the pre-fit is assigned to the CPE and its capacitor value  $C_1$  is used as start value for  $Q$  (See Equation 1). Because the exponent of the CPE cannot be assigned, it is always set to  $n = 0.75$ . The component  $R_{ct}$  receives the resistance value  $R_1$  from the same RC element. The

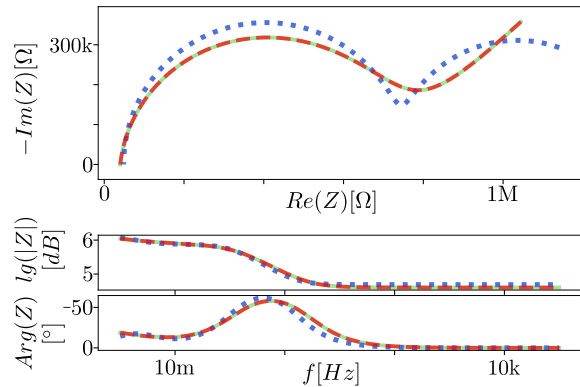


Figure 3: Exemplary illustration of a simulated spectrum (green) with the result of the pre-fit (blue) and the corresponding result of the CNLS (red) in the Nyquist and Bode plot.

second RC element and  $Z_w$  are handled in the same way.

In the investigations of this work, a normal CNLS is performed first, whose start values are the logarithmic means of the defined ranges. If this does not lead to a satisfying result, the same is done with a former pre-fitting, which is exemplarily shown in Figure 3.

### 2.3 Elliptical Fitting

In case only the parameter  $R_{ct}$  is of interest for sensor analysis, a geometric approach based on elliptical fitting was developed. Here it is taken into account that the influence of the Warburg impedance is only effective at comparably low frequencies. In higher frequency ranges, the equivalent circuit results in the parallel circuit  $R_{ct}||CPE$  shifted by the series resistor  $R_s$ . Since this parallel circuit leads to a semicircle or a depressed semicircle (Orazem and Tribollet, 2008) (Shoar Abouzari et al., 2009) with characteristic points in the Nyquist plot (see Figure 4), an elliptical fitting can be used to extract the value of  $R_{ct}$ .

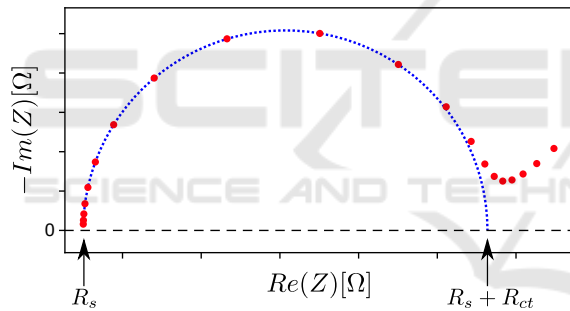


Figure 4: Exemplary Nyquist plot of a simulated data set from a Randles circuit (red) with a fitted semicircle (blue). The left zero crossing of the semicircle represents the  $R_s$ , the remaining zero crossing describes  $R_s + R_{ct}$ .

In order to suppress the influence of the Warburg impedance at lower measuring frequencies and thus not to distort the fitting of the ellipse, a pre-selection of measuring points is made. Only measuring points on the semicircle at the Nyquist plot should be used. The turning point between semicircle and Warburg impedance is used as the cut-off point. To find this point a 5th degree polynomial is fitted to the impedance values of the Nyquist plot. This polynomial degree has proven to be a good value to avoid overfitting, but still to reproduce the curve as accurately as possible. Starting from the polynomial, the first and second derivatives are formed. The inflection point now results from the zero point of the second derivative, as far as the first derivative is positive. All points to the left of this point are used for the ellipse

fit.

When a cone is cut on a plane that does not contain the apex or is perpendicular to the axis of rotation, an ellipse is obtained. A circle is only a special case of an ellipse with half axes of equal size. For this reason the basis for the fit is the general cone equation

$$F(\vec{a}, \vec{x}) = ax^2 + bxy + cy^2 + dx + ey + f = 0. \quad (12)$$

Hereby,  $\vec{a} = [a \ b \ c \ d \ e \ f]^T$  and  $\vec{x} = [x^2 \ xy \ y^2 \ x \ y \ 1]^T$  (Fitzgibbon et al., 1999). The algebraic distance  $F(a, x)$  is the distance of a point  $(x, y)$  from the intersection edge  $F(a, x) = 0$ . Using the method of least squares this distance shall be minimized for given data points. To avoid trivial solutions like  $\vec{a} = 0$  additional conditions have to be set to the solution. A simple approach is the consideration as an eigenvalue problem. For this a quadratic condition matrix  $C$  is set up. The eigenvalue problem thus results in

$$D^T Da = \lambda Ca \quad (13)$$

with the design matrix  $D = [x_1 \ x_2 \ c \dots \ x_n]^T$  (Bookstein, 1979).  $C$  has the condition that the vector  $\vec{a}$  must describe an ellipse. Fitzgibbon et al. described that this can be achieved with a negative discriminant  $b^2 - 4ac$  (Fitzgibbon et al., 1999). This is generally difficult to solve, but this application leaves the freedom to scale the parameters arbitrarily. Thus the equality constraint  $4ac - b^2 = 1$  is obtained. In matrix notation the constraint can be written as

$$\vec{a}^T C \vec{a} = 1 \quad (14)$$

where

$$C = \begin{bmatrix} 0 & 0 & 2 & 0 & 0 & 0 \\ 0 & -1 & 0 & 0 & 0 & 0 \\ 2 & 0 & 0 & 0 & 0 & 0 \\ 0 & 0 & 0 & 0 & 0 & 0 \\ 0 & 0 & 0 & 0 & 0 & 0 \\ 0 & 0 & 0 & 0 & 0 & 0 \end{bmatrix}. \quad (15)$$

The minimization problem can then be solved by calculating the eigenvectors of the Equation 13. If now a pair of eigenvalue and eigenvector  $(\lambda_i, \vec{u}_i)$  solves the equation system, so does also  $(\lambda_i, \mu \vec{u}_i)$  with each value of  $\mu$ . With the condition from Equation 14 we can now find a value for  $\mu$  thus resulting in

$$\mu_i^2 \vec{u}_i^T C \vec{u}_i = 1. \quad (16)$$

Accordingly, it applies that

$$\mu_i = \sqrt{\frac{1}{\vec{u}_i^T C \vec{u}_i}} \quad (17)$$

The parameters for an ellipse, which solves the optimization problem, now result from

$$\hat{a}_i = \mu_i \vec{u}_i. \quad (18)$$

### 3 RESULTS

Both approaches, the CNLS and the elliptical fitting were applied to the simulated spectra. An exemplary data set is shown in Figure 5.

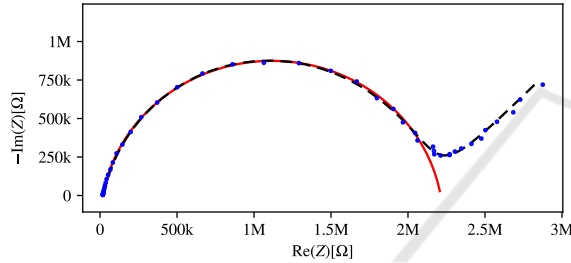


Figure 5: Example of simulated data points of a Randles circuit with superimposed noise (blue;  $R_s = 1.72 \cdot 10^4$ ,  $R_{ct} = 2.10 \cdot 10^6$ ,  $Q_w = 2.83 \cdot 10^{-7}$ ,  $Q = 3.13 \cdot 10^{-10}$ ,  $n = 0.88$ ), the appropriate result of the model fitting (black;  $-0.05\%$  error of the  $R_{ct}$  calculation) and of the elliptical fitting (red,  $0.26\%$  error of the  $R_{ct}$  calculation).

The calculated value of the parameter  $R_{ct}$  were extracted and compared to the original value of the simulation. They were used to calculate the mean relative error  $E_R$  and the coefficient of determination  $R^2$ . The simulated spectra, which could not be fit by one of the presented approaches, were discarded for further investigation. The raw and noisy data were considered separately. To compare the performance of both approaches, the required calculation times were measured for each fitting procedure. All methods are implemented in the Python programming language. The simulations were performed on a 1.90 GHz Intel® Core™ i7-8650U Processor with 16 GB of RAM.

The achieved results for both methods are shown in Table 2. The relative Error  $E_R$  represents the difference between the calculated value  $R_{ct,c}$  and the true value  $R_{ct,t}$ , referred to  $R_{ct,t}$ . The linear relationship  $R_{ct,c} = mR_{ct,t} + b$  with its coefficient of determination  $R^2$  were calculated and is exemplary shown in Figure 6 for the noisy spectra. Table 2 also shows the number of discarded spectra  $N_d$  which could not be fitted with the presented approaches.

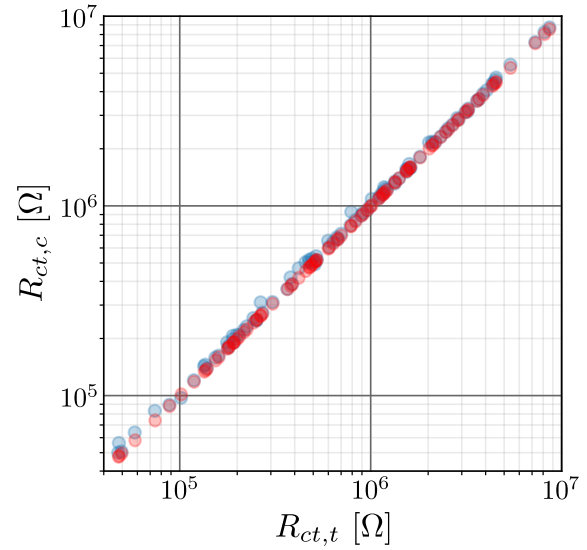


Figure 6: Linear relationship between the calculated values  $R_{ct,c}$  of the CNLS (red) or the elliptical fitting (blue) and the true value  $R_{ct,t}$ .

The calculation time for each approach was measured, whereby all steps depending on the method (e.g. preselection of measuring points, normalization, fitting) were included. The distribution of the calculation times is shown as boxplot for the raw spectra in Figure 7.

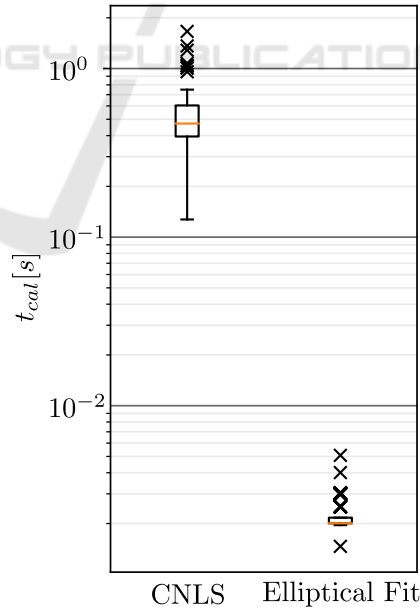


Figure 7: Distribution of the calculation time for CNLS and the elliptical fitting. 100 raw spectra without noise were used.

Table 2: Results of the simulation of the CNLS and the elliptical fitting  $EF$ . Raw signals ( $CNLS_r, EF_r$ ) and noisy signals ( $CNLS_n, EF_n$ ) were observed. The parameters mean relative error  $E_R$ , slope  $m$ , intercept  $b$ , coefficient of determination  $R^2$ , number of discarded spectra  $N_d$ , median calculation time  $t_{cal}$  were determined.

	$E_R[\%]$	$m$	$b[\Omega]$	$R^2$	$N_d$	$t_{cal}[s]$
$CNLS_r$	$1.5 \cdot 10^{-6} \pm 1.5 \cdot 10^{-5}$	1.00000	$1.2 \cdot 10^{-3}$	1.00000	1	$4.6 \cdot 10^{-1}$
$EF_r$	$-2.7 \pm 4.2$	1.01027	$5.6 \cdot 10^3$	0.99957	2	$2.0 \cdot 10^{-3}$
$CNLS_n$	$2.4 \cdot 10^{-2} \pm 4.6 \cdot 10^{-1}$	0.99934	$5.3 \cdot 10^2$	0.99997	0	$4.5 \cdot 10^{-1}$
$EF_n$	$-2.7 \pm 4.3$	1.00965	$5.6 \cdot 10^3$	0.99950	2	$2.0 \cdot 10^{-3}$

## 4 DISCUSSION AND OUTLOOK

By using the CNLS, low error in the calculation of  $R_{ct}$  is achieved and also the linear relationship to the real value is better compared to the elliptical fitting at least for non-noisy spectra. However, this difference in performance is smaller when considering noisy spectra. This observation leads to the assumption that for very noisy signals the difference between the two approaches could become even smaller. However, this has to be investigated and evaluated in the following work, preferably by using real measured spectra from FET-based biosensors. Besides the consideration of different noise overlays, the analysis of artifact influences would also be relevant.

The results of the time measurements show that the elliptical fitting is more resource efficient than CNLS. However, these results have to be interpreted in the context of the normalization that has been carried out for the CNLS. In this process, all components of the equivalent circuit diagram are replaced by a factor  $a$  and an exponent  $b$  (see Equation 9), which in turn makes the regression more time-consuming. Nevertheless, the elliptical fitting might be more suitable to be implemented on low-power embedded systems. In this respect, further concepts have to be developed how this approach can be efficiently implemented on an embedded system. Thus an investigation of the power consumption would be applicable as well.

Although the elliptical fitting requires less computational time than the CNLS, it is also able to fit the majority of the spectra within the data set considered in this work, which in turn stands for a high robustness of the algorithm. However, the CNLS with the pre-fit algorithm achieves even better results but with a greater computational effort. It should be emphasized that the pre-fit was mainly responsible for achieving these good values, since without the pre-fit the CNLS would have had to reject 33 spectra (without noise) or respective 31 spectra (with noise). It is also striking that the superimposed noise has a positive effect on the modeling ability of the CNLS,

although a strong vulnerability to noise has already been described in the literature (Kauffman, 2009). The results also confirm that start values of the components are decisive for the error obtained with CNLS and demonstrate the effectiveness of the pre-fit algorithm. However, the disadvantage of a high dependency on the start values applies less strongly to the elliptical fitting. Nevertheless, further optimizations of the elliptical fitting should be implemented, allowing to reliably fit more spectra. This can be achieved by intercepting cases where the Warburg impedance already dominates at the imaginary maximum of the semicircle, causing the pre-selection of measurement points to be erroneous.

For a real application scenario, the presented approaches should be adapted in order to optimize their performance. For example, due to smaller min-max limits of the individual parameters, particular exponents can be fixed so that the regression is less computationally demanding. However, the presented approaches allow the modelling of a wide range of parameter combinations without the need to specify approximate initial values or narrower limits for extreme values. They thus represent generic modelling techniques.

In cases where  $C_{dl}$  can be applied instead of  $CPE$ , the semicircle of the Randles circuit is not depressed. For this purpose, further research is needed to determine the accuracy and computational effort that can be achieved by a circular fitting.

## 5 SUMMARY

With an average error of  $-2.7\%$ , the elliptical fitting cannot achieve the accuracy of the CNLS ( $2.4 \cdot 10^{-2}\%$ ) for the determination of  $R_{ct}$ , at least when using ideal spectra. Thereby it could be shown that pre-fit is a suitable method to reduce the dependence of CNLS on the start value. Preliminary data indicate that the results of elliptical fitting are less dependent on noise than CNLS, but in any case, the lat-

ter has lower errors and a lower number of rejected spectra for the data used in this work. However, this behavior needs further investigation. The measurements of the computation time showed that the elliptical fitting needs only about  $1/225$  of the computational effort compared to the CNLS. This leads to the assumption that this approach might be suitable for implementations on embedded systems. For this purpose the accuracy of the elliptical fitting has to be estimated depending on the application, the measurement and/or the sensor.

## ACKNOWLEDGEMENTS

This research was funded by EU H2020 research and innovation program entitled KardiaTool with grant N° 768686.

## REFERENCES

- Barsoukov, E. and Macdonald, J. R. (2005). *Impedance Spectroscopy: Theory, Experiment, and Applications*.
- Barsoukov, Y. and Macdonald, J. R. (2012). *Electrochemical Impedance Spectroscopy*, pages 1–17. American Cancer Society.
- Bertsekas, D. P. (1999). *Nonlinear programming, Second Edition*.
- Bookstein, F. L. (1979). Fitting conic sections to scattered data. *Computer Graphics and Image Processing*.
- Chowdhury, A. D., Ganganboina, A. B., Park, E. Y., and an Doong, R. (2018). Impedimetric biosensor for detection of cancer cells employing carbohydrate targeting ability of Concanavalin A. *Biosensors and Bioelectronics*.
- Cimafonte, M., Fulgione, A., Gaglione, R., Papaianni, M., Capparelli, R., Arciello, A., Censi, S. B., Borriello, G., Velotta, R., and Ventura, B. D. (2020). Screen printed based impedimetric immunosensor for rapid detection of Escherichia coli in drinking water. *Sensors (Switzerland)*.
- Dang, W., Manjakkal, L., Navaraj, W. T., Lorenzelli, L., Vinciguerra, V., and Dahiya, R. (2018). Stretchable wireless system for sweat pH monitoring. *Biosensors and Bioelectronics*.
- Fitzgibbon, A., Pilu, M., and Fisher, R. B. (1999). Direct least square fitting of ellipses. *IEEE Transactions on Pattern Analysis and Machine Intelligence*.
- Halima, H. B., Zine, N., Gallardo-Gonzalez, J., Aissari, A. E., Sigaud, M., Alcacer, A., Bausells, J., and Er-rachid, A. (2019). A Novel Cortisol Biosensor Based on the Capacitive Structure of Hafnium Oxide: Application for Heart Failure Monitoring. In *20th International Conference on Solid-State Sensors, Actuators and Microsystems and Eurosensors*.
- Kauffman, G. B. (2009). *Electrochemical Impedance Spectroscopy*. By Mark E. Orazem and Bernard Tribollet. *Angewandte Chemie International Edition*.
- Kharitonov, A. B., Wasserman, J., Katz, E., and Willner, I. (2001). The use of impedance spectroscopy for the characterization of protein-modified ISFET devices: Application of the method for the analysis of biorecognition processes. *Journal of Physical Chemistry B*.
- Leva-Bueno, J., Peyman, S. A., and Millner, P. A. (2020). A review on impedimetric immunosensors for pathogen and biomarker detection. *Medical Microbiology and Immunology*.
- Macdonald, D. D. (1990). Some advantages and pitfalls of electrochemical impedance spectroscopy. *Corrosion*.
- Orazem, M. E. and Tribollet, B. (2008). *Electrochemical Impedance Spectroscopy*. Wiley.
- Papageorgiou, M., Leibold, M., Buss, M., Papageorgiou, M., Leibold, M., and Buss, M. (2015). Methode der kleinsten Quadrate. In *Optimierung*.
- Pejčić, B. and De Marco, R. (2006). Impedance spectroscopy: Over 35 years of electrochemical sensor optimization. *Electrochimica Acta*.
- Prodromidis, M. I. (2010). Impedimetric immunosensors-A review. *Electrochimica Acta*.
- Randviir, E. P. and Banks, C. E. (2013). Electrochemical impedance spectroscopy: An overview of bioanalytical applications. *Analytical Methods*, 5(5):1098–1115.
- Rushworth, J. V., Ahmed, A., Griffiths, H. H., Pollock, N. M., Hooper, N. M., and Millner, P. A. (2014). A label-free electrical impedimetric biosensor for the specific detection of Alzheimer’s amyloid-beta oligomers. *Biosensors and Bioelectronics*.
- Sgobbi, L. F., Razzino, C. A., and Machado, S. A. (2016). A disposable electrochemical sensor for simultaneous detection of sulfamethoxazole and trimethoprim antibiotics in urine based on multiwalled nanotubes decorated with Prussian blue nanocubes modified screen-printed electrode. *Electrochimica Acta*.
- Shoar Abouzari, M. R., Berkemeier, F., Schmitz, G., and Wilmer, D. (2009). On the physical interpretation of constant phase elements. *Solid State Ionics*, 180(14-16):922–927.
- Sun, A., Venkatesh, A. G., and Hall, D. A. (2016). A Multi-Technique Reconfigurable Electrochemical Biosensor: Enabling Personal Health Monitoring in Mobile Devices. *IEEE Transactions on Biomedical Circuits and Systems*.
- Willa, C., Schmid, A., Briand, D., Yuan, J., and Koziej, D. (2017). Lightweight, Room-Temperature CO<sub>2</sub> Gas Sensor Based on Rare-Earth Metal-Free Composites - An Impedance Study. *ACS Applied Materials and Interfaces*.
- Yuan, X.-Z., Song, C., Wang, H., and Zhang, J. (2010). *Electrochemical Impedance Spectroscopy in PEM Fuel Cells*. Springer, London.